# Numerical investigation of the influence of electron beam acceleration voltage in powder based additive manufacturing processes

**Fuad Osmanlic, Alexander Klassen, Thorsten Scharowsky, Carolin Körner**

*Powder-bed based additive manufacturing with selective electron beam melting is a highly complex process. Determining the parameters for good quality parts is of prime importance. To identify the process window, the process is modeled at a mesoscopic scale. The full set of equations for thermo- and hydrodynamics is solved, considering most notably phase change, electron beam absorption with depth-dose profiles, free surface movement and stochastic powder particle distribution. The influence of an increase in electron beam acceleration voltage from commercially available 60 kV to 120 kV on consolidation of the powder is investigated by numerical means. An improvement of consolidation behavior by an extension of the processing window is demonstrated numerically for Ti-6Al-4V. Thus, the potential for higher acceleration voltages for future machine design is shown.*

***Числено изследване на влиянието на ускоряващото напрежение на електронния сноп в адитивни (с добавяне на метал) процеси, базирани на използването на метални прахове (Фуад Османлик, Александър Класен, Торстен Чаровски, Каролин Коернер).*** *Адитивното производство, в което се използва добавяне на метал и прахово ложе със селективно топене с електронен лъч е изключително сложен процес. Изборът на параметрите на процеса за получаване на добро качество на получаваните детайли е от първостепенно значение. За идентифициране прозореца на процеса, процесът се моделира в мезоскопичен мащаб. Пълният набор от топло- и хидро-динамични уравнения е решен, като се има предвид най-вече фазовите промени, поглъщането на електрони с профили «дълбочина доза», свободното движение на повърхността и стохастичното разпределение на праховите частици. Влиянието на нарастване на ускоряващото напрежение на електронния сноп от търговски достъпното 60 kV до 120 kV за консолидацията на праха се изследва с числени средства. Едно подобрение на поведението на консолидация чрез разширяване на прозореца на обработка се демонстрира числено за Ti-6Al-4V. По този начин, е показан потенциалът за използване на по-високи ускоряващи напрежения при бъдещо проектиране на машини за адитивно производство с добавяне на метални прахове.*

## Introduction

Selective electron beam melting (SEBM) is an additive manufacturing technology mainly governed by physical phenomena such as electron beam absorption, rapid local heating and cooling, surface tension forces in combination with wetting effects between the melt and the loosely packed powder bed, thermal cycling and evaporation. These play a critical role in affecting the quality of the final product. It is of most importance to determine the scanning parameters for a stable process window to produce dense and near net-shape parts. In this numerical study, the influence of beam acceleration voltage on the process window is investigated.

## Numerical model

In the present work, numerical analysis of the SEBM process is performed employing the lattice Boltzmann method (LBM). The LBM is a rapidly developing alternative approach to traditional computational fluid dynamics (CFD) and has its strengths in the simulation of multi-phase flows involving complex geometries. The coupled hydrodynamic and thermodynamic behavior of metal powder irradiated by an intense electron beam can be

represented by the following system of equations,

$$(1)\quad \nabla \cdot \mathbf{u} = 0,$$

$$(2)\quad \frac{\partial \mathbf{u}}{\partial t} + (\mathbf{u}\cdot\nabla)\mathbf{u} = -\frac{1}{\rho}\nabla p + \frac{\mu}{\rho}\nabla^2\mathbf{u} + \mathcal{S}_{\mathrm{F}},$$

$$(3)\quad \frac{\partial h_{\mathrm{E}}}{\partial t} + \mathbf{u}\cdot\nabla h_{\mathrm{E}} = \nabla\left(\frac{\lambda}{\rho c_{\mathrm{p}}}\cdot\nabla h_{\mathrm{E}}\right) + \mathcal{S}_{\mathrm{H}},$$

where (1) is the continuity equation, (2) are the incompressible Navier-Stokes equations and (3) is the convection-diffusion equation. Here, $\mathbf{u}$ is the local fluid velocity vector, $t$ is the time, $p$ is the pressure, $\mu$ is the dynamic viscosity, $h_{\mathrm{E}}$ is the specific enthalpy and $\lambda/\rho c_{\mathrm{p}}$ is the thermal diffusivity, with the thermal conductivity $\lambda \equiv \lambda(h_{\mathrm{E}})$ and the specific heat capacity $c_{\mathrm{p}} \equiv c_{\mathrm{p}}(h_{\mathrm{E}})$. The external source terms, $\mathcal{S}$, account for effects like gravitational acceleration and recoil pressure due to evaporation ($\mathcal{S}_{\mathrm{F}}$) and electron beam absorption as well as evaporative energy losses to the surroundings ($\mathcal{S}_{\mathrm{H}}$).

The fundamental basis of the LBM is that, in the limit of small Mach and Knudsen numbers, the discrete Boltzmann equation is formally equivalent to the incompressible Navier-Stokes equations [1]. Rigorous theoretical treatments of the lattice Boltzmann method can be found in the literature [2]-[5]. The LBM used here is based on a two-dimensional single phase free surface method developed at the Chair of Materials Science and Engineering for Metals, University of Erlangen-Nuremberg, Germany **Error! Reference source not found.**. The numerical model can solve hydrodynamic flow [7], electron beam absorption [8], heat conduction, melting and solidification [9] and single component evaporation [10].

In contrast to laser beams, the electron energy absorbed per unit length reaches its peak value at a significant distance from the target surface, requiring an electron beam model that rests on a volumetric approach rather than a surface heat source. The absorption characteristics of electrons incident on a target can be accurately described by depth-dose profiles, the calculation of which is based on a set of semi-empirical equations. More details are to be found in [8]. Depth-dose profiles are treated as a function of the acceleration voltage, the target material and the angle of beam incidence. Two such profiles are shown in Fig. 1, where the absorbed electron energy in the titanium alloy Ti–6Al–4V is plotted for two different acceleration voltages, *i.e.*, 60 kV and 120 kV. Here, for 60 kV, the depth of maximum energy dissipation is about 4 µm and the penetration depth is 18 µm. For 120 kV, corresponding values are 13 µm and 54 µm, respectively.

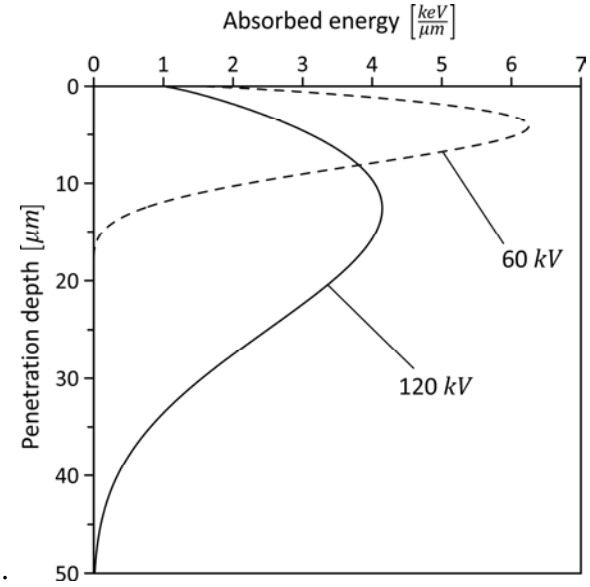


*Fig. 1. Depth-dose profiles in Ti–6Al–4V at 60 kV and 120 kV acceleration voltage and normal beam incidence.*

**Experimental and numerical setup**

All experiments presented in this work were conducted on an Arcam S12 machine using Ti–6Al–4V powder. The system consists of an evacuated building tank with an adjustable process platform and a rake system to apply powder. The electron gun was operated at a constant acceleration voltage of 60 kV having a maximum power of 3 kW.

The specimens were produced in three steps. First, the powder was applied to the building platform and heated with the defocused beam up to approximately 700 °C. At this temperature the powder sinters and produces a stable powder bed for melting. In the next step, the focused beam scans a square area of 15 mm x 15 mm with a given scanning strategy. Here, the area is scanned with lines having an offset of $l_{\mathrm{off}} = 100$ µm. Every second line the beam scanning vector changes into the opposite direction (Fig. 2, left). This so called “snake” hatching is one of the most common scanning strategies when fabricating bulk components and was therefore chosen for this study. After the melting step, the platform was lowered by 50 µm and a new powder layer was applied. In the experiments, the beam velocity $v_{\mathrm{beam}}$ was varied between 0.5 m/s and 6.4 m/s and the beam power $P_{\mathrm{beam}}$ between 150 W and 2000 W.

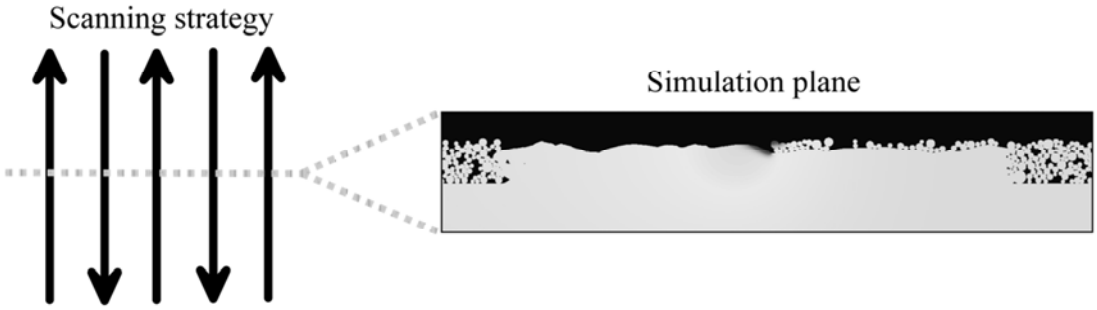


*Fig. 2. (left) Schematic illustrating the scanning strategy using "snake"-like hatching, where arrows represent the scan path of the electron beam. The build direction is out-of-plane. (right) 2D simulation plane showing the temperature field at an instant in time. The position of the simulation plane with respect to the scan direction is indicated by the dashed line*

The 2D simulation plane lies in the center of the scanning area, parallel to the build direction and perpendicular to the scan path of the electron beam (Fig. 2, dashed lines). The space and time discretization is set to $\Delta x = 5$ µm and $\Delta t = 2 \cdot 10^{-7}$ s. Table 1 shows the physical properties of the titanium alloy Ti–6Al–4V used for the numerical computations.

For the electron beam, a Gaussian beam power distribution is assumed with a beam diameter ($4\sigma$) of 400 µm. A process window with an acceleration voltage of 60 kV is simulated and compared with the experimental findings. To study the effect of increasing the acceleration voltage to 120 kV, a second process window is calculated with the same parameters.

**Table 1**

*Physical properties of Ti–6Al–4V.*

| | |
|---|---|
| density | 4122 kg/m³ [11] |
| dyn. viscosity | 4.76 mPa s [12] |
| surface tension | 1.52 J/m² [12] |
| specific heat (solid) | 670 J/kg/K [13] |
| specific heat (liquid) | 1126 J/kg/K [13] |
| solidus temperature | 1878 K [14] |
| liquidus temperature | 1928 K [14] |
| boiling temperature | 3315 K [15] |
| latent heat of fusion | 290 kJ/kg [13] |
| latent heat of vaporization | 9820 kJ/kg [16] |

For the electron beam, a Gaussian beam power distribution is assumed with a beam diameter ($4\sigma$) of 400 µm. A process window with an acceleration voltage of 60 kV is simulated and compared with the experimental findings. To study the effect of increasing the acceleration voltage to 120 kV, a second process window is calculated with the same parameters.

**Results**

The experimental and numerical results are shown in Fig. 3. For the produced specimens, a simple classification according the relative density and the surface quality is employed. Three classes are distinguished, *i.e.*, porous, good and wavy. Porous samples have a relative density lower than 0.995, where 1.0 is the full density of Ti–6Al–4V. Wavy means that the top surface of the parts has a wavy structure and therefore is no longer considered near net-shape. These surface structures are a result of the melt flow induced by recoil pressure, which is caused by the evaporating mass. Therefore, the mass loss is a suitable measure for comparing experimental and simulation results. Note that the loss of mass can also lead to significant deviations in the chemical composition of the alloy in the presence of volatile elements. Good samples are considered between those two limits. The lower limit is given by the porosity and the upper limit by the loss of mass due to evaporation.

In Fig. 3a, the simulated relative density map at 60 kV is plotted along with experimental data. It is found that the 0.995 isoline is between the good and porous samples. This demonstrates the excellent agreement between predicted and measured data. Furthermore, Fig. 3b contains the mass loss map at 60 kV, which indicates that the critical evaporated mass, separating samples with a wavy surface from those with a plane surface, is 0.12 g for this particular setup. The maps for the relative density and the mass loss for an acceleration voltage of 120 kV are shown in Fig. 3c and Fig. 3d. In both cases, the process window is enlarged as compared to the 60 kV electron beam.

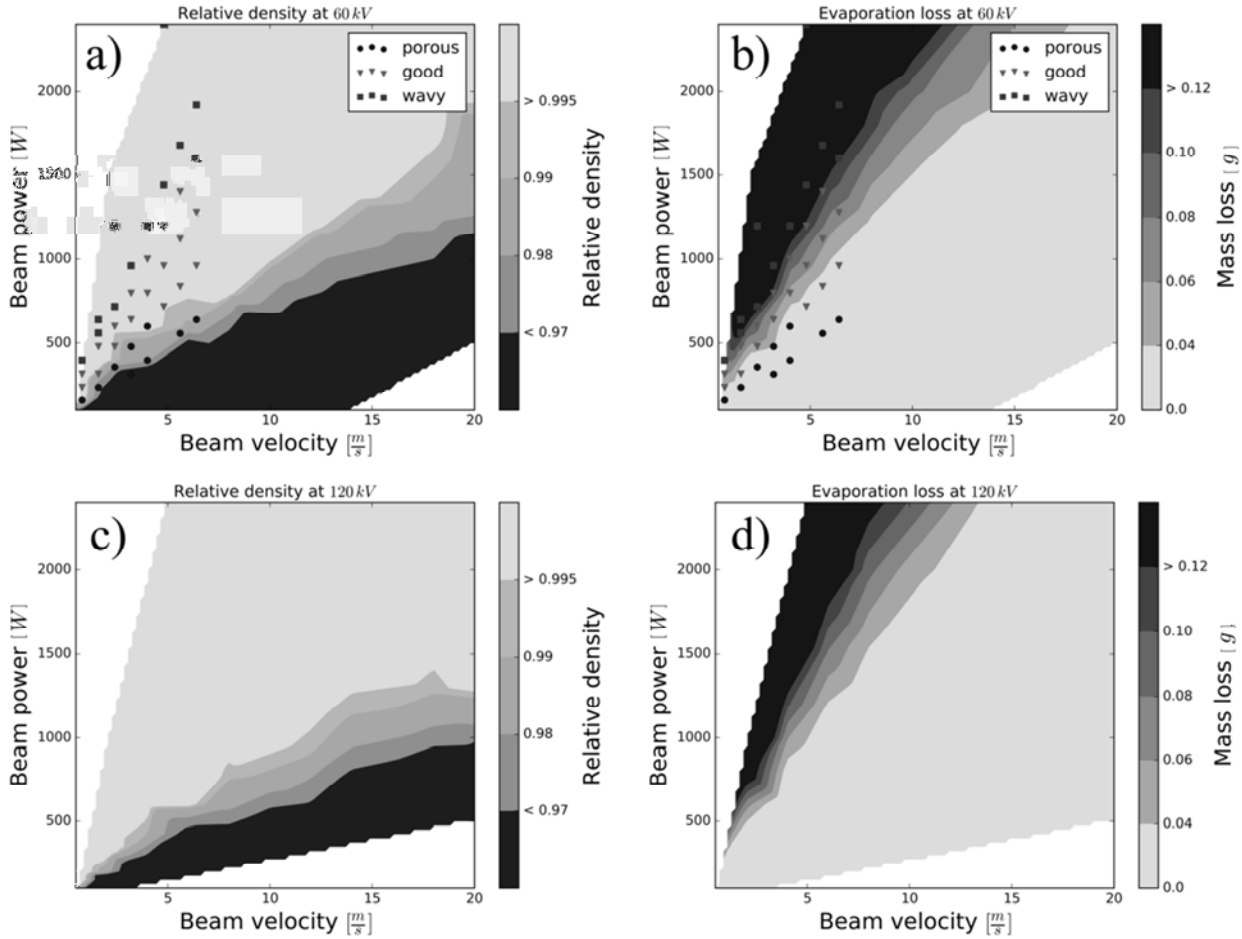


*Fig. 3. a) Relative density map and b) Mass loss map at 60 kV. Data points represent experiments. c) Relative density map and d) Mass loss map at 120 kV*

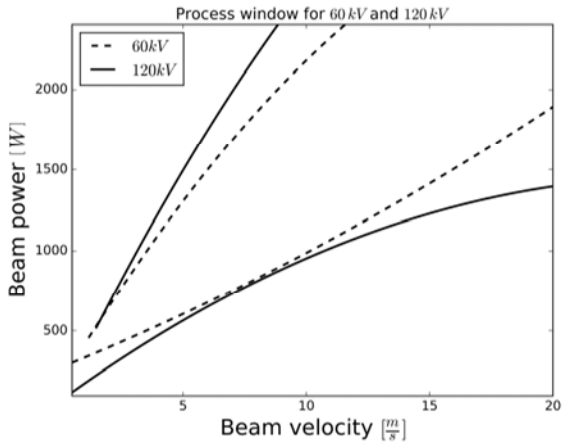


*Fig. 4. Comparison of the process windows for 60 kV and 120 kV*

The process windows at 60 kV and 120 kV, represented by smooth isolines for the upper and lower bounds, are shown in Fig. 4. It is seen that the process window is wider at an acceleration voltage of 120 kV, especially at higher beam velocities and beam powers.

## Conclusions

The conducted numerical study indicates that doubling the acceleration voltage from 60 kV to 120 kV extends the process window in terms of porosity and evaporative mass loss. The process window opens even further at higher velocities and beam powers, thereby making it possible to increase the building rate, while producing dense near net-shape parts having a constant chemical composition. Therefore, electron guns with higher acceleration voltages should be considered for future machine designs.


## Acknowledgements

The authors gratefully acknowledge funding of the German Research Council (DFG) within the Collaborative Research Center 814 ‘Additive Manufacturing’, project B4.

**REFERENCES**


[1] X. He, L.-S. Luo. Lattice Boltzmann model for the incompressible Navier-Stokes equation. J Stat Phys, 1997, 88:927-944.

[2] S. Chen, G. D. Doolen. Lattice Boltzmann method for fluid flows. Annu Rev Fluid, 1998, 30:329-364.

[3] P. Lallemand, L.-S. Luo. Theory of the lattice Boltzmann method: Dispersion, dissipation, isotropy, Galilean invariance, and stability. ICASE Report 2000-17, 2000.

[4] S. Succi. The lattice Boltzmann equation for fluid dynamics and beyond. Oxford: Clarendon Press, 2000.

[5] D. d'Humières, I. Ginzburg, M. Krafczyk, P. Lallemand, L.-S. Luo. Multiple-relaxation-time lattice Boltzmann models in three dimensions. Philos Trans R SocLond, Ser A, 2002, 360:437-451.

[6] C. Körner, M. Thies, T. Hofmann, N. Thürey, U. Rüde. Lattice Boltzmann model for free surface flow for modeling foaming. J Stat Phys, 2005, 121:179-196.

[7] E. Attar, C. Körner. Lattice Boltzmann method for dynamic wetting problems. J Colloid Interface Sci, 2009, 335:84-93.

[8] A. Klassen, A. Bauereiß, C. Körner. Modelling of electron beam absorption in complex geometries. J Phys D: Appl Phys, 2014, 47:065307.

[9] E. Attar, C. Körner. Lattice Boltzmann method for thermal free surface flows with liquid-solid phase transition. Int J Heat Fluid Fl, 2011, 32:156-163.

[10] A. Klassen, T. Scharowsky, C. Körner. Evaporation model for beam based additive manufacturing using free surface lattice Boltzmann methods. J Phys D: Appl Phys, 2014, 47:275303.

[11] J. J. Z. Li, W. L. Johnson, W.-K. Rhim. Thermal expansion of liquid Ti-6Al-4V measured by electrostatic levitation. Appl Phys Lett, 2006, 89:111913.

[12] R. K. Wunderlich. Surface tension and viscosity of industrial Ti-alloys measured by the oscillating drop method on board parabolic flights. High Temp Mater Process, 2008, 27:401-412.

[13] M. Boivineau, C. Cagran, D. Doytier, V. Eyraud, M.-H. Nadal, B. Wilthan, G. Pottlacher. Thermophysical properties of solid and liquid Ti-6Al-4V (TA6V) alloy. Int J Thermophys, 2006, 27:507-529.

[14] R. Boyer, G. Welsch, E. W. Collings. Materials Properties Handbook: Titanium Alloys. Materials Park, OH: ASM International, 1998, p. 513.

[15] R. Rai, P. Burgardt, J. O. Milewski, T. J. Lienert, T. DebRoy. Heat transfer and fluid flow during electron beam welding of 21Cr-6Ni-9Mn steel and Ti-6Al-4V alloy. J Phys D: Appl Phys, 2009, 42:025503.

[16] T. Iida, R. I. L. Guthrie. The Physical Properties of Liquid Metals. Oxford: Clarendon, 1988.



***Fuad Osmanlic*** *- Address: Chair of Materials Science and Engineering for Metals, University of Erlangen-Nuremberg, Martensstr. 5, D-91058 Erlangen, Germany;*

*Tel.: +49 (0)9131 8527527;*

*Fax: +49 (0)9131 8527515;*

*E-mail: fuad.osmanlic@fau.de*

***Alexander Klassen*** *- Chair of Materials Science and Engineering for Metals, University of Erlangen-Nuremberg;*

*E-mail: alexander.klassen@fau.de*

***Thorsten Scharowsky*** *- Chair of Materials Science and Engineering for Metals, University of Erlangen-Nuremberg;*

*E-mail: thorsten.scharowsky@fau.de*

***Prof. Dr.-Ing. habil. Carolin Körner*** *- Chair of Materials Science and Engineering for Metals, University of Erlangen-Nuremberg;*

*E-mail: carolin.koerner@fau.de*